

Pulsatile Flow Around 3-Dimensionally Curved Arteries for Varying Body Mass

Jonathan Mestel

Leszek Zabielski

Imperial College London

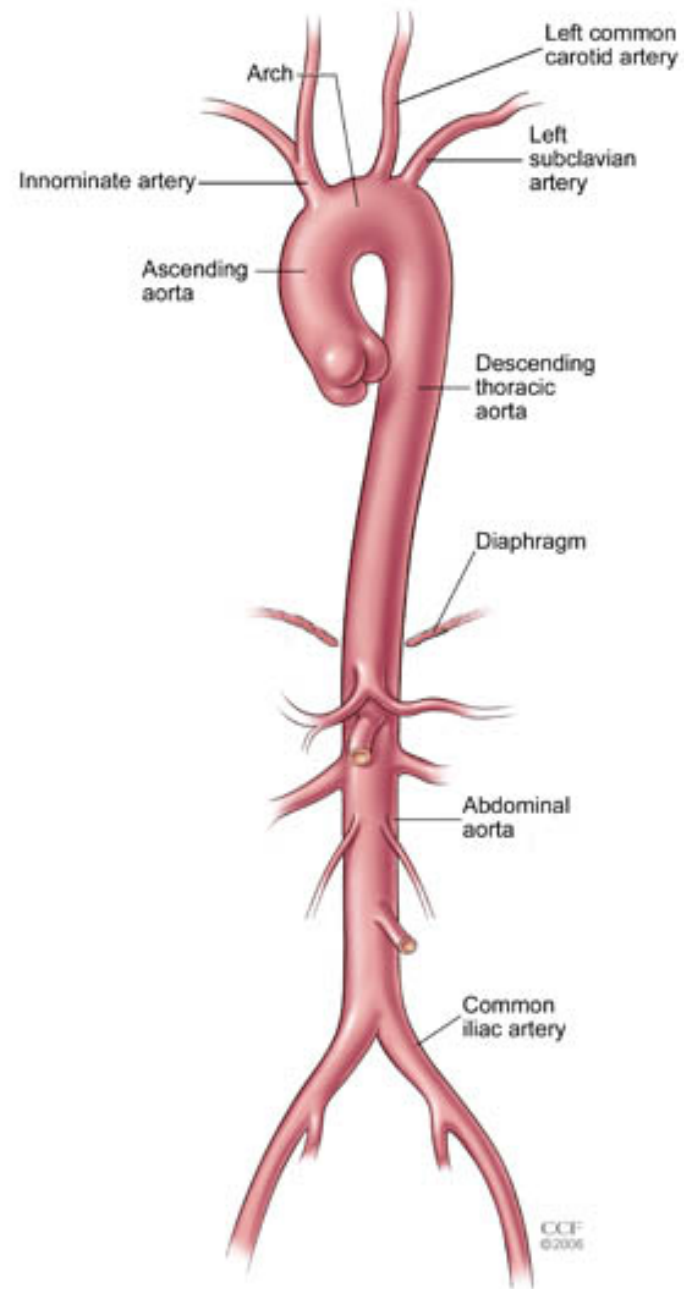
Warsaw University of Technology

Bio Fluid Mechanics, Lecture 18

Outline

- **Motivation**
- **Allometric model: isotropic**
- **Anisotropic aorta scalings**
- **Computations for helical flow**
- **Conclusions**

Physiological background



Physiological background

Arteries are observed to curve three-dimensionally. Caro et al (1971, 1996) suggested this might give rise to fluid dynamics less prone to the development of atheroma. We concentrate today on the aortic arch over a range of animal sizes.

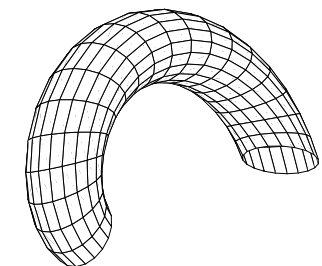
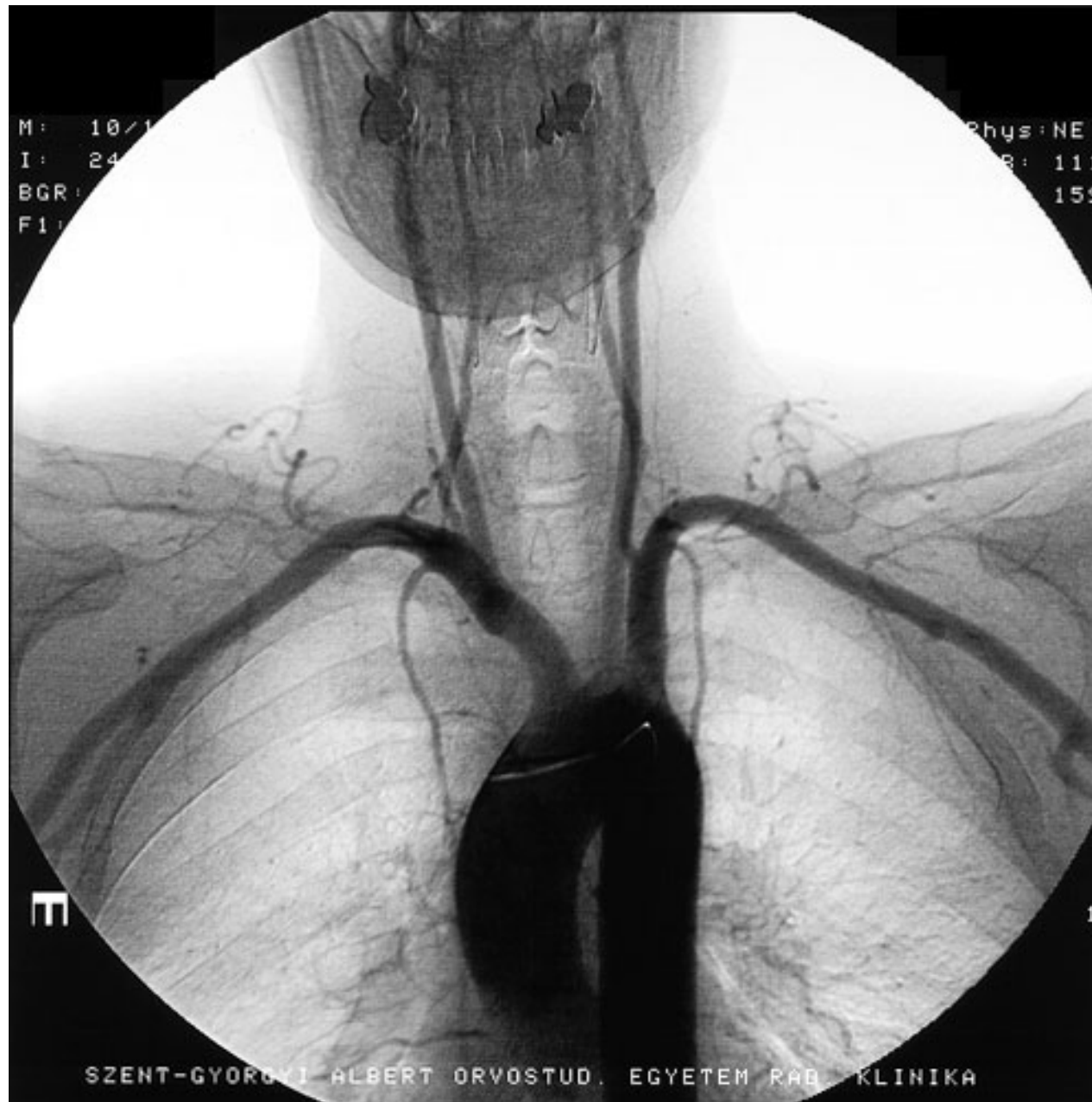
Zabielski & Mestel (1998,2000) investigated effects of arterial torsion using a helical model. We revisit and revise this work.

Rigid walls, no branches, fully developed, Newtonian flow.

The aortic arch



The aortic arch



Really helical arteries – the umbilical cord



The driving pressure gradient

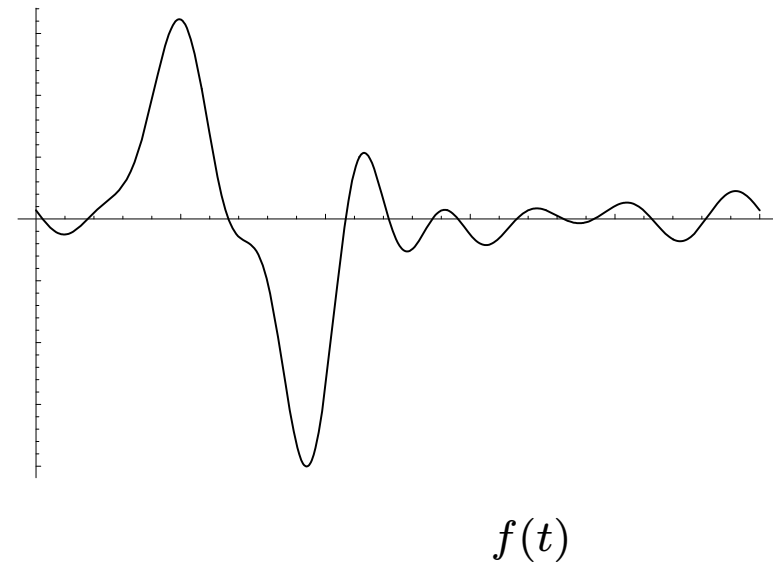
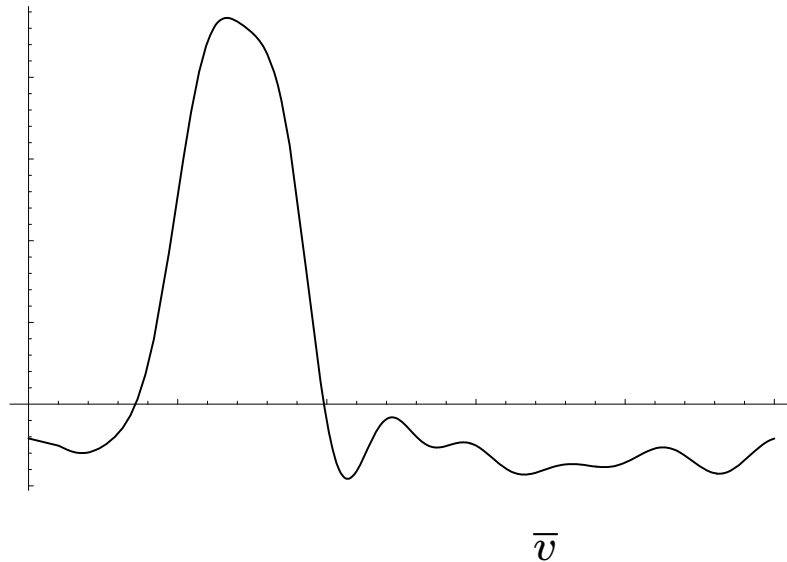
Suitably non-dimensionalised, the down-pipe N-S equation takes the form

$$\alpha^2 \frac{\partial v}{\partial t} + \mathbf{u} \cdot \nabla v = R + R_s \alpha^3 f(t) + \nabla^2 v + \text{curvature terms}$$

where α is the Womersley number $\alpha = (\omega_0 a^2 / \nu)^{1/2}$ and R and R_s are the amplitudes of the steady and fluctuating parts. The pulse shape $f(t)$ is obtained from measurements and is assumed to be exactly periodic, and the same for all subjects.

For given geometry and pulse shape, the problem depends on 3 parameters. We aim to use allometric arguments to select suitable parameter values for numerical calculation.

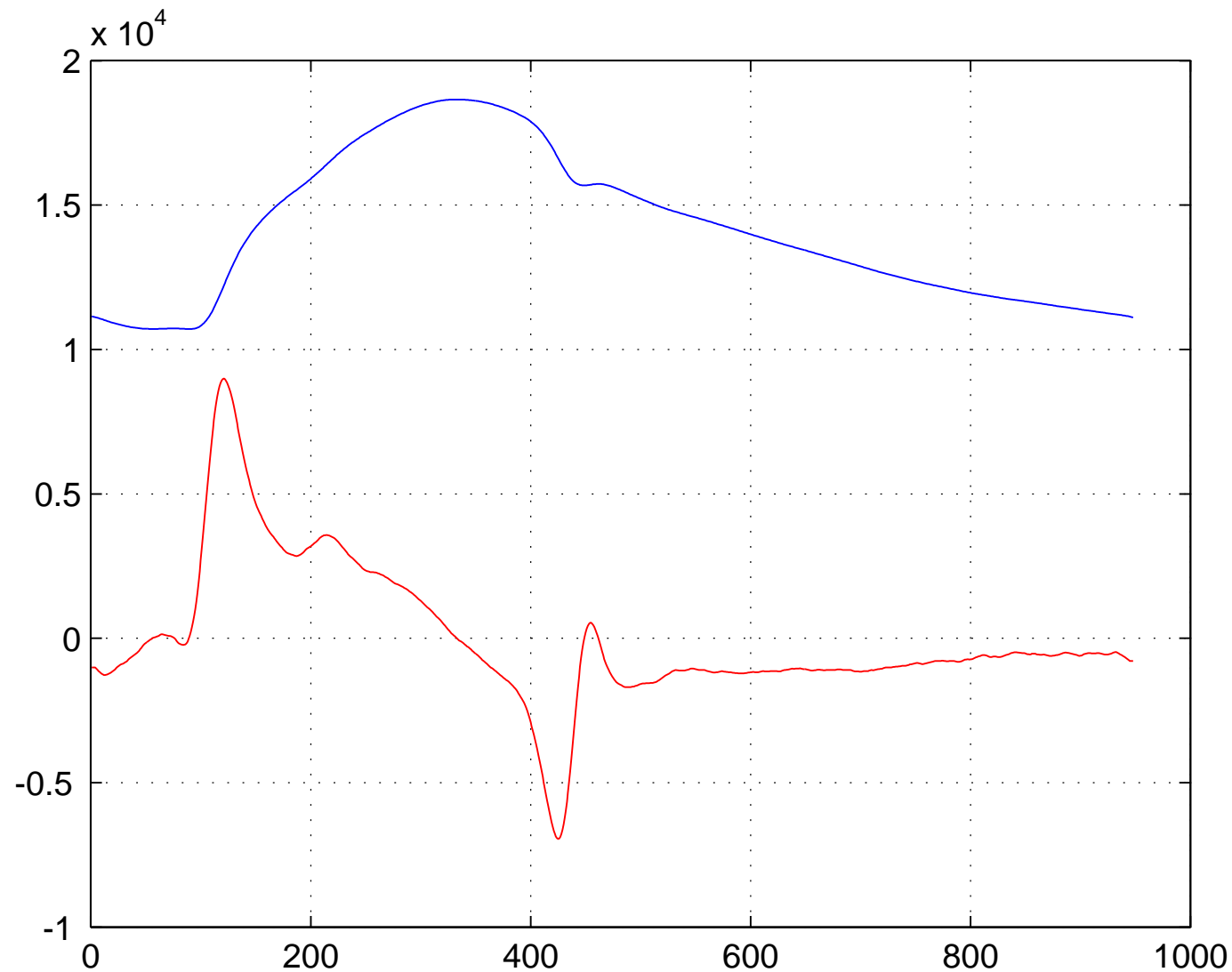
Canine pressure gradient



Measured velocity profile and pressure gradient from Parker (2000), used in isotropic model.

Pressure gradient for elderly human

Data for **Pressure** and **Pressure gradient** from Parker (2007) used in anisotropic calculations.



An allometric model (isotropic)

Consider a class of geometrically similar animals, characterised by a single length-scale, or equivalently, its mass M . Assume quantities depend on M as a power law, for example:

$$\text{Aorta volume} \propto M \quad \Longrightarrow \quad \text{Aorta radius } a \propto M^{1/3}$$

assuming aorta shape is the same for all sizes.

An allometric model (isotropic)

Consider a class of geometrically similar animals, characterised by a single length-scale, or equivalently, its mass M . Assume quantities depend on M as a power law, for example:

$$\text{Aorta volume} \propto M \quad \Longrightarrow \quad \text{Aorta radius } a \propto M^{1/3}$$

assuming aorta shape is the same for all sizes.

Metabolic rate $\propto M^{3/4}$ **The mouse to elephant curve**

Oxygen supply suggests that heart frequency

$$\omega_0 \propto M^{-1/4} \quad \Longrightarrow \quad \alpha = \left(\frac{\omega_0 a^2}{\nu} \right)^{1/2} \propto M^{5/24} \simeq M^{0.21}$$

An allometric model (isotropic)

How does R scale with M ?

The cardiac output is expected to scale as

$$Q \propto M^{3/4} \propto \pi a^2 \bar{v} \implies \bar{v} \propto M^{1/12}$$

For steady flow, at high Reynolds (Dean) number R , can estimate the velocity scale

$$\bar{v} \propto \frac{\nu}{a} R^{2/3}$$

which leads to

$$R \propto M^{5/8} = M^{0.625}$$

An allometric model (isotropic)

How does R_s scale with M ?

Balancing as in Womersley flow

$$\text{unsteady pressure gradient} \sim \frac{\partial v}{\partial t}$$

leads to the scaling

$$v' \propto \frac{\alpha R_s}{a}$$

Using empirical result that $v' \propto \bar{v}$ ($v' \simeq 5 \times \bar{v}$) we deduce

$$R_s \propto M^{5/24}$$

An allometric model (isotropic)

In fact, if we modify these scalings using empirical data from Stahl (1968) and Pedley (1978) giving $Q \propto M^{0.81}$ rather than $M^{0.75}$ we obtain the values (M in kg):

$$R_s = 84.8 \times M^{0.27}, \quad \alpha^2 = 57 \times M^{0.42}, \quad R = 1140 \times M^{.65}$$

Pipe curvature and torsion independent of M .

These values, given in the following table, were used in the numerical calculations of ZM2000

(Zabielski & Mestel J. Biomech. Eng. 122 (2000)):

Scalings for isotropic aortas

	$M [kg]$	diameter in cm	α (Womersley)	R'	R'_s
mouse	0.017	0.16 (0.07)	3.20 (1.5)	40.9	28.2
rat	0.6	0.52 (0.2)	6.78 (3.3)	410	73.8
ferret	1.5	0.71 (0.3)	8.22 (3.7)	741.6	94.6
rabbit	3	0.90 (0.34)	9.50 (4.0)	1161	114
cat	4	0.98 (0.4)	10.1 (4.4)	1398	123
	10	1.33	12.24	2529	158
	15	1.52	13.33	3287	176
dog	20	1.68 (1.56)	14.16 (13.1)	3959	190
	30	1.92	15.42	5146	212
	40	2.12	16.38	6198	230
	50	2.28	17.16	7161	244
	60	2.42	17.83	8056	256
man	75	2.62 (3)	18.70 (22.2)	9307	272
ox	500	4.92 (4)	27.84 (25.6)	31740	454
horse	850	5.87 (7.6)	31.12 (41.8)	44740	524
elephant	2000	7.81 (9)	37.25 (49.2)	77800	660

In brackets, experimental data for the proximal aorta from McDonald.

These values suggest altering the scaling law for aortic radius and Womersley number.

Anisotropic model

Weinberg & Ethier (2007) and Greve et al (2007) suggest that the aorta does not scale isotropically. Rather, its radius a and length b may obey (West et al 1997)

$$a \propto M^{3/8} \quad b \propto M^{1/4}$$

This means the pipe curvature increases with size

$$\delta \equiv \frac{a}{b} \propto M^{1/8}$$

We will assume the pipe torsion increases at the same rate so that the helical parameter

$$\varepsilon \propto M^{1/8}$$

Note pipe intersects itself for $\delta > 1$. ($M > 30$ tons.)

Anisotropic model

$$a \propto M^{3/8} \quad b \propto M^{1/4} \quad \varepsilon \propto M^{1/8}$$

Cardiac output scaling as $Q \propto M^{3/4}$ leads to a mean velocity independent of size

$$\bar{v} \propto M^0$$

Anisotropic model

$$a \propto M^{3/8} \quad b \propto M^{1/4} \quad \varepsilon \propto M^{1/8}$$

The Womersley number

$$\alpha \propto a\omega_0^{1/2} \propto M^{3/8}M^{-1/8} = M^{1/4} \quad (M^{5/24} \text{ before})$$

Anisotropic model

$$a \propto M^{3/8} \quad b \propto M^{1/4} \quad \varepsilon \propto M^{1/8}$$

The Womersley number

$$\alpha \propto a\omega_0^{1/2} \propto M^{3/8}M^{-1/8} = M^{1/4} \quad (M^{5/24} \text{ before})$$

Peak velocity v' is also observed to be independent of size (about 1m/s) so

$$\frac{\alpha R_s}{a} \propto v' \quad \implies \quad R_s \propto M^{1/8} \quad (M^{5/24} \text{ before})$$

Anisotropic model

$$a \propto M^{3/8} \quad b \propto M^{1/4} \quad \varepsilon \propto M^{1/8}$$

The Womersley number

$$\alpha \propto a\omega_0^{1/2} \propto M^{3/8}M^{-1/8} = M^{1/4} \quad (M^{5/24} \text{ before})$$

Peak velocity v' is also observed to be independent of size (about 1m/s) so

$$\frac{\alpha R_s}{a} \propto v' \quad \Longrightarrow \quad R_s \propto M^{1/8} \quad (M^{5/24} \text{ before})$$

High Dean number steady flow

$$\bar{v} \propto \frac{\nu}{a} R^{2/3} \quad \Longrightarrow \quad R \propto M^{9/16} \quad (M^{5/8} \text{ before})$$

Scaling of Wall Shear Stress

Until fairly recently (Weinberg & Ethier 2007), experimental physiologists believed that

- the blood velocity, V , was independent of size
- the wall shear stress, $\tau \sim \mu V/L$, was independent of size.

These two statements are clearly incompatible with a size-dependent length-scale! While it isn't obvious whether L should scale with a , a/α or some other boundary layer thickness, it is mathematically obvious that τ decreases with M if V is constant. The manner in which endothelial (wall) cells respond to stress needs thus to be rethought.

Helical blood flow

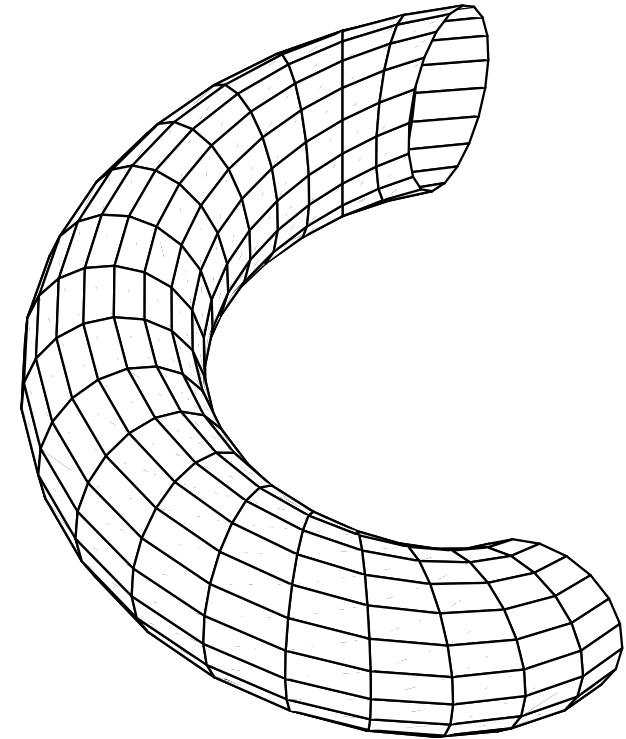
- Laminar, incompressible flow is driven down a rigid helical pipe of circular cross-section driven by a
- measured, physiological pressure profile, assumed time-periodic and the same shape for all animal sizes.
- Helical symmetry is imposed on the velocity field.
- Fully developed nonlinear solutions are found numerically. These are usually time-periodic.
- Problem depends on 5 parameters, chosen allometrically as described before.

Helical symmetry

In terms of cylindrical polar coordinates (r, θ, z) ,
the helical symmetry direction \mathbf{H} is given by

$$\mathbf{H} = \frac{1}{h^2}(-\varepsilon r \mathbf{e}_\theta + \mathbf{e}_z) \quad h = (1 + \varepsilon^2 r^2)^{1/2}$$

\mathbf{e}_θ and \mathbf{e}_z are unit vectors in the θ and z directions.
The constant ε measures the pitch of a given helical line.



Helical pipe

$$\varepsilon a = 1 \quad b/a = 2.5$$

Helical symmetry

In terms of cylindrical polar coordinates (r, θ, z) ,
the helical symmetry direction \mathbf{H} is given by

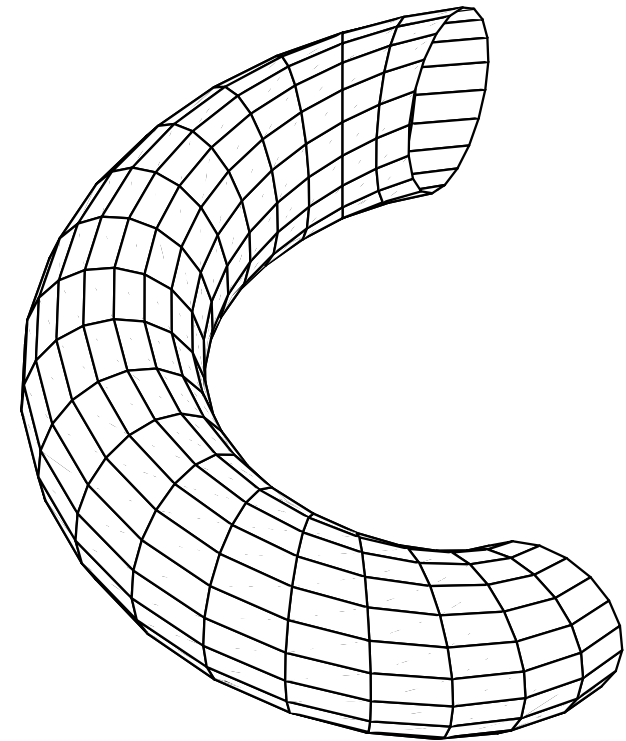
$$\mathbf{H} = \frac{1}{h^2}(-\varepsilon r \mathbf{e}_\theta + \mathbf{e}_z) \quad h = (1 + \varepsilon^2 r^2)^{1/2}$$

\mathbf{e}_θ and \mathbf{e}_z are unit vectors in the θ and z directions.
The constant ε measures the pitch of a given helical line.

\mathbf{H} is a non-unit Beltrami field

$$\nabla \times \mathbf{H} = -\frac{2\varepsilon}{h^2} \mathbf{H},$$

This Beltrami property is responsible
for genuinely three-dimensional behaviour.



Helical pipe

$$\varepsilon a = 1 \quad b/a = 2.5$$

Helical symmetry

In terms of cylindrical polar coordinates (r, θ, z) ,
the helical symmetry direction \mathbf{H} is given by

$$\mathbf{H} = \frac{1}{h^2}(-\varepsilon r \mathbf{e}_\theta + \mathbf{e}_z) \quad h = (1 + \varepsilon^2 r^2)^{1/2}$$

\mathbf{e}_θ and \mathbf{e}_z are unit vectors in the θ and z directions.
The constant ε measures the pitch of a given helical line.

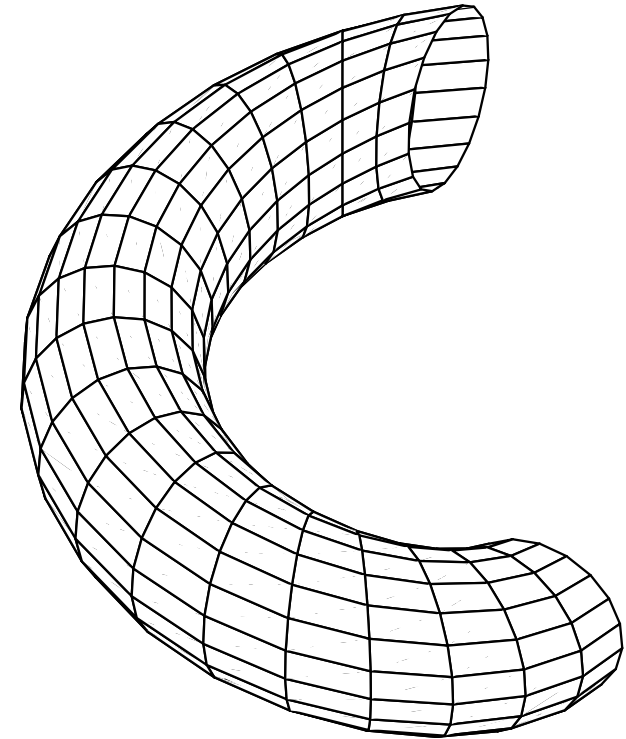
\mathbf{H} is a non-unit Beltrami field

$$\nabla \times \mathbf{H} = -\frac{2\varepsilon}{h^2} \mathbf{H},$$

This Beltrami property is responsible
for genuinely three-dimensional behaviour.

A scalar function f is helically symmetric when

$$f = f(r, \phi) \quad \phi = \theta + \varepsilon z$$



Helical pipe

$$\varepsilon a = 1 \quad b/a = 2.5$$

Helical symmetry

In terms of cylindrical polar coordinates (r, θ, z) ,
the helical symmetry direction \mathbf{H} is given by

$$\mathbf{H} = \frac{1}{h^2}(-\varepsilon r \mathbf{e}_\theta + \mathbf{e}_z) \quad h = (1 + \varepsilon^2 r^2)^{1/2}$$

\mathbf{e}_θ and \mathbf{e}_z are unit vectors in the θ and z directions.
The constant ε measures the pitch of a given helical line.

\mathbf{H} is a non-unit Beltrami field

$$\nabla \times \mathbf{H} = -\frac{2\varepsilon}{h^2} \mathbf{H},$$

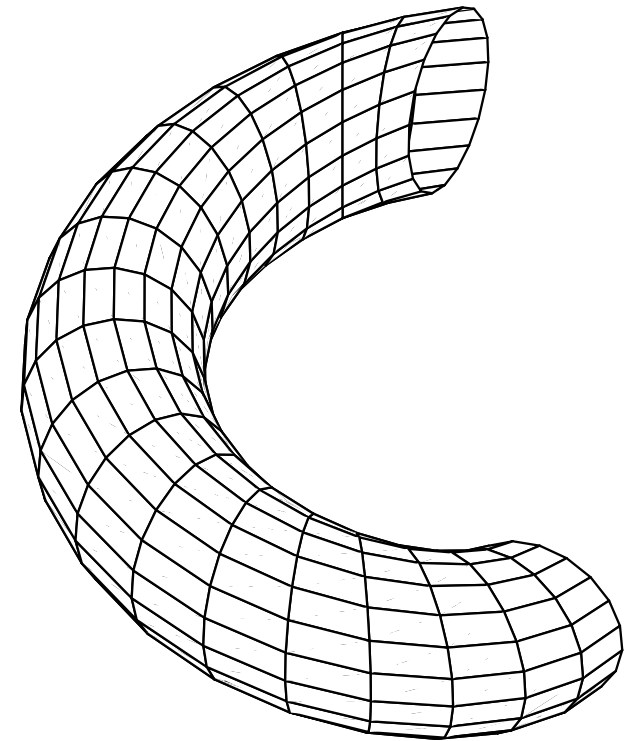
This Beltrami property is responsible
for genuinely three-dimensional behaviour.

A scalar function f is helically symmetric when

$$f = f(r, \phi) \quad \phi = \theta + \varepsilon z$$

In the limits $\varepsilon \rightarrow 0 \Rightarrow \mathbf{H} \rightarrow \mathbf{e}_z$,
 $\varepsilon \rightarrow \infty \Rightarrow h\mathbf{H} \rightarrow -\mathbf{e}_\theta$

so that helical symmetry simplifies to
two-dimensionality ($\varepsilon = 0$) and axisymmetry ($\varepsilon \rightarrow \infty$).



Helical pipe

$$\varepsilon a = 1 \quad b/a = 2.5$$

Helical representation of the velocity field

Helically symmetric solenoidal velocity field:

$$\mathbf{u} = \mathbf{H} \times \nabla \Psi + v \mathbf{H}$$

The vorticity vector field $\boldsymbol{\omega} = \nabla \times \mathbf{u}$

$$\boldsymbol{\omega} = \mathbf{H} \times \nabla(-v) + \xi \mathbf{H} \quad \text{where } \mathcal{L}\Psi = \frac{2\varepsilon}{h^2}v + \xi.$$

Navier-Stokes equations:

$$\frac{\partial v}{\partial t} + \frac{1}{r} J(\Psi, v) = G(t) + \nu(\mathcal{L}v + \frac{2\varepsilon}{h^2}\xi)$$

$$\frac{\partial \xi}{\partial t} + \left(-\frac{2\varepsilon}{h^2} \frac{1}{r} J(\Psi, v) + \frac{1}{r} J(\Psi, \xi) + \frac{2\varepsilon^2}{h^2} \left(\xi \frac{\partial \Psi}{\partial \phi} + v \frac{\partial v}{\partial \phi} \right) \right) = \nu(\mathcal{L}\xi - \frac{2\varepsilon}{h^2}(\mathcal{L}v + \frac{2\varepsilon}{h^2}\xi))$$

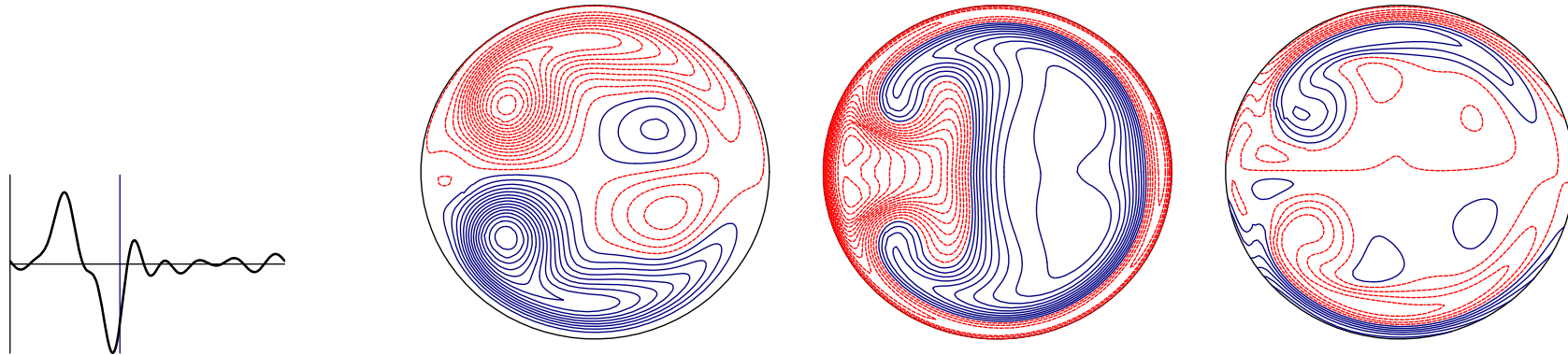
$G(t)$ is the imposed down-pipe pressure gradient, $G = \alpha^{-2}R + R_s\alpha f(t)$.

In this talk, G is assumed periodic with a measured physiological profile $f(t)$.

The amplitudes R , R_s and frequency α^2 are determined allometrically.

Numerical solutions for isotropic scaling

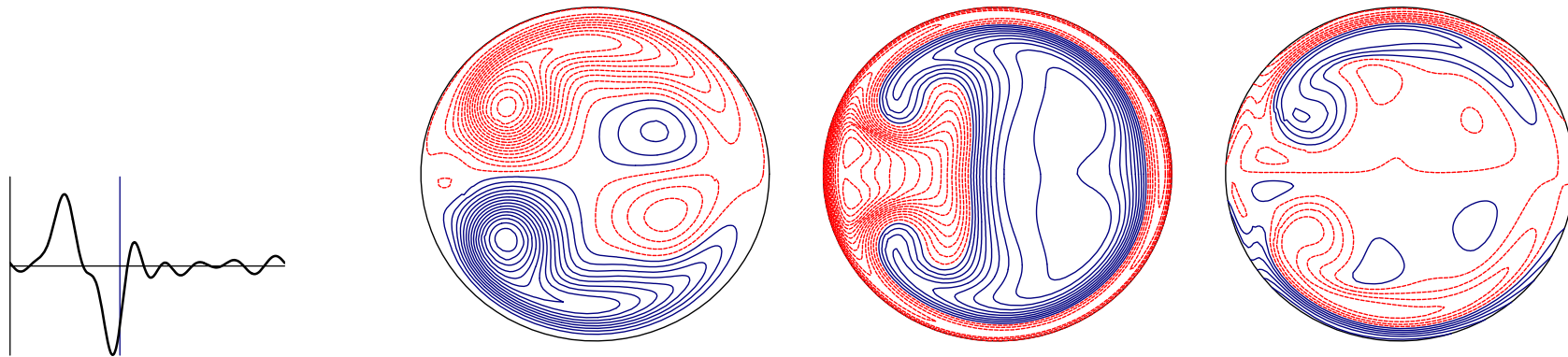
The effect of the helical bend: The advantage of a 3-D bend can be seen from this animation of the flow which would occur in a 3kg rabbit with a planar aortic bend:



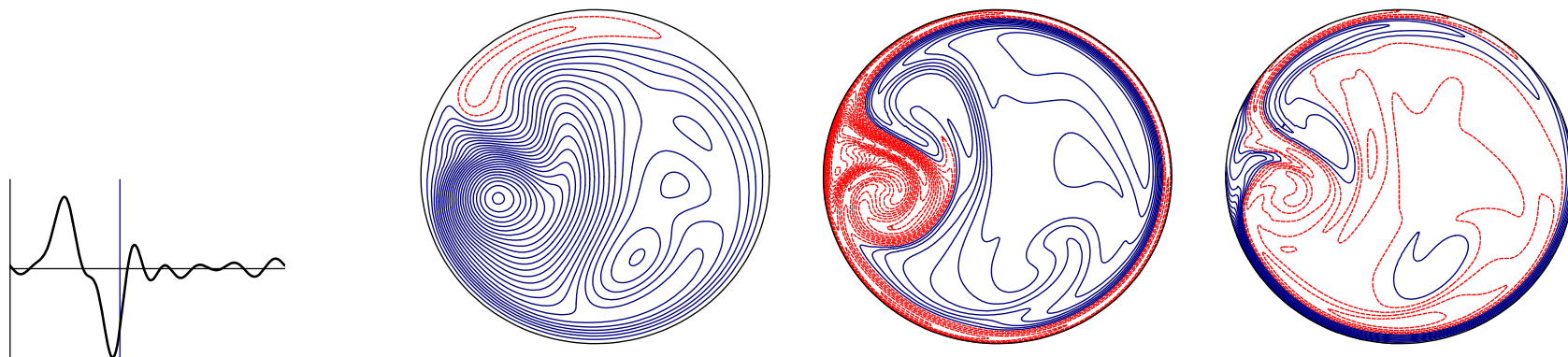
Animations: Ferret $M = 1.5$ Dog $M = 20$

Numerical solutions for isotropic scaling

The effect of the helical bend: The advantage of a 3-D bend can be seen from this animation of the flow which would occur in a 3kg rabbit with a planar aortic bend:



In contrast the separation at the inside of a helical bend is more benign, even for a 60kg man:



Animations: Ferret $M = 1.5$ Dog $M = 20$

Numerical solutions for anisotropic case

General behaviour: At lower values of M the flow is gentler, and has the same time period as the pressure. During systole the flow can resemble a quasistatic two-vortex Dean flow, but the single vortex helical flow dominates during diastole. Back flow is greater than in the isotropic case.

Animations:

rat, $M = 0.6$

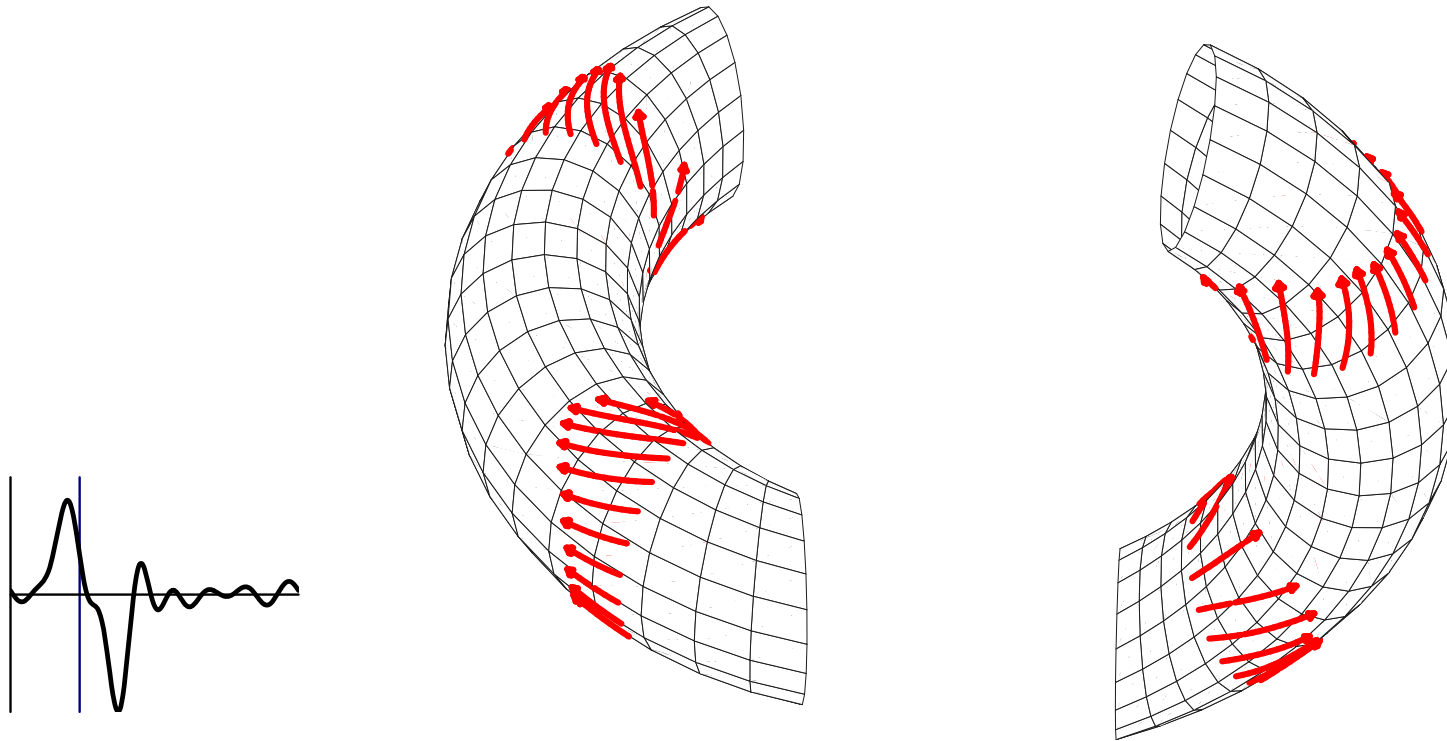
rabbit, $M = 3$

dog, $M = 20$

man $M = 75$

Wall shear distribution for a 20kg dog

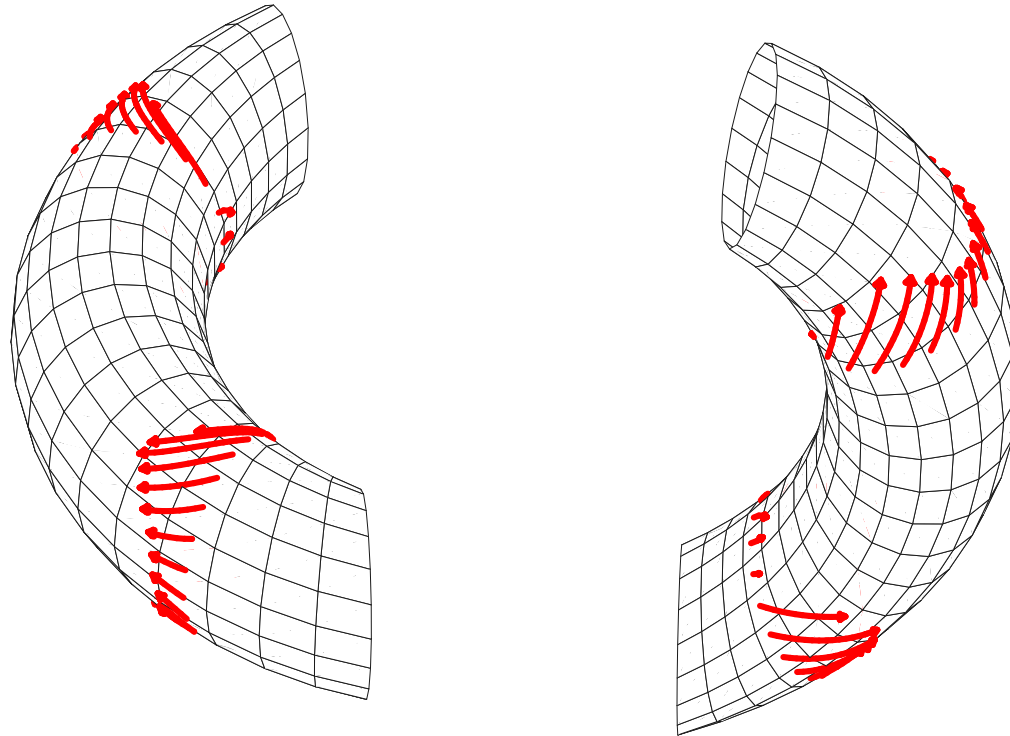
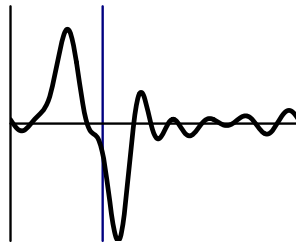
(a)



Wall shear on the boundary of a helical bend $\varepsilon = 1$, $b = 2.5$.
Flow conditions as for the canine aortic arch with $M = 20$.

Wall shear distribution for a 20kg dog

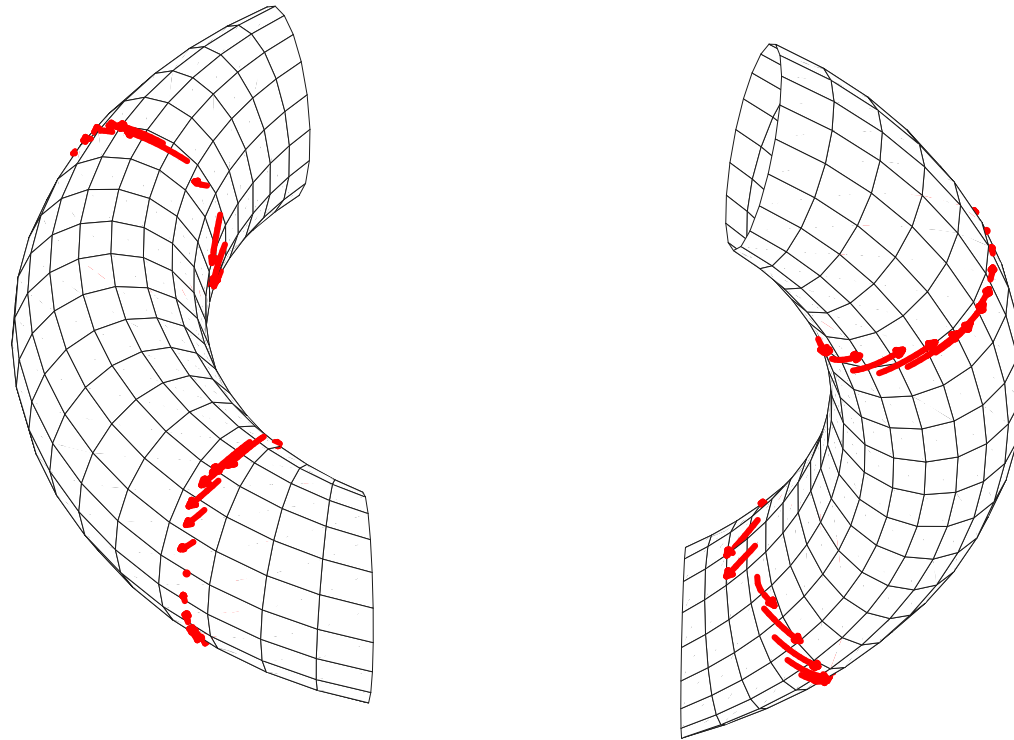
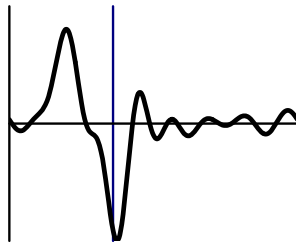
(b)



Wall shear on the boundary of a helical bend $\varepsilon = 1$, $b = 2.5$.
Flow conditions as for the canine aortic arch with $M = 20$.

Wall shear distribution for a 20kg dog

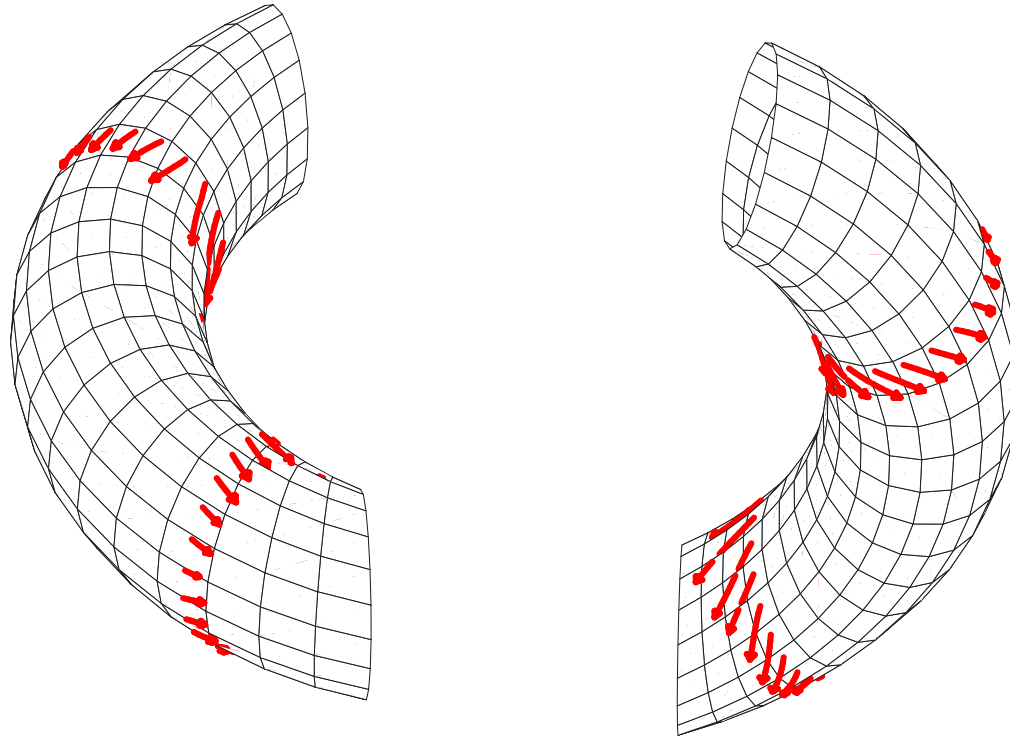
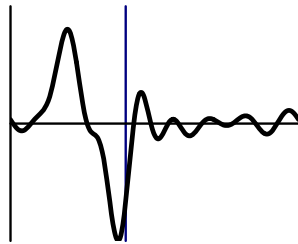
(c)



Wall shear on the boundary of a helical bend $\varepsilon = 1$, $b = 2.5$.
Flow conditions as for the canine aortic arch with $M = 20$.

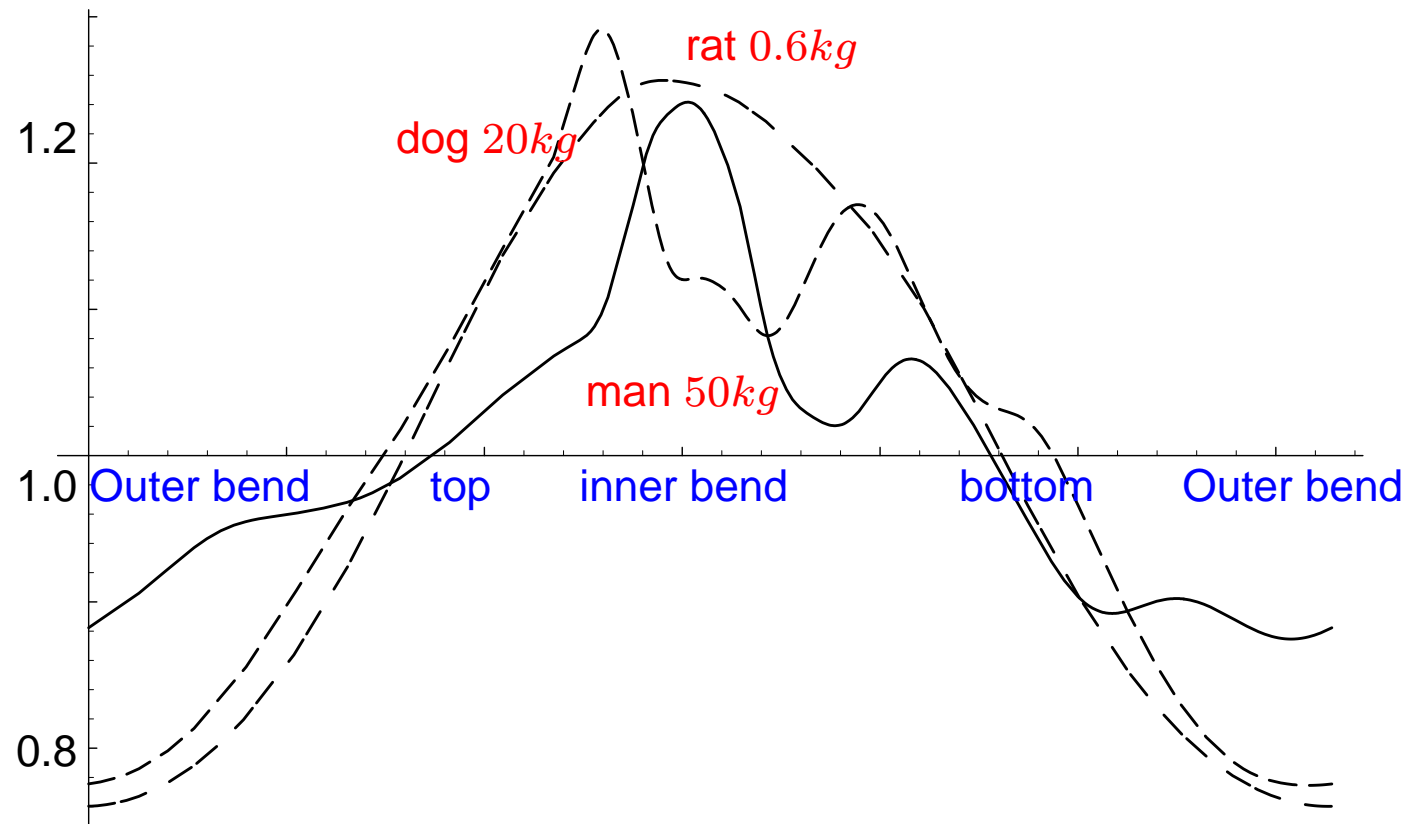
Wall shear distribution for a 20kg dog

(d)



Wall shear on the boundary of a helical bend $\varepsilon = 1$, $b = 2.5$.
Flow conditions as for the canine aortic arch with $M = 20$.

Wall shear spatial distribution

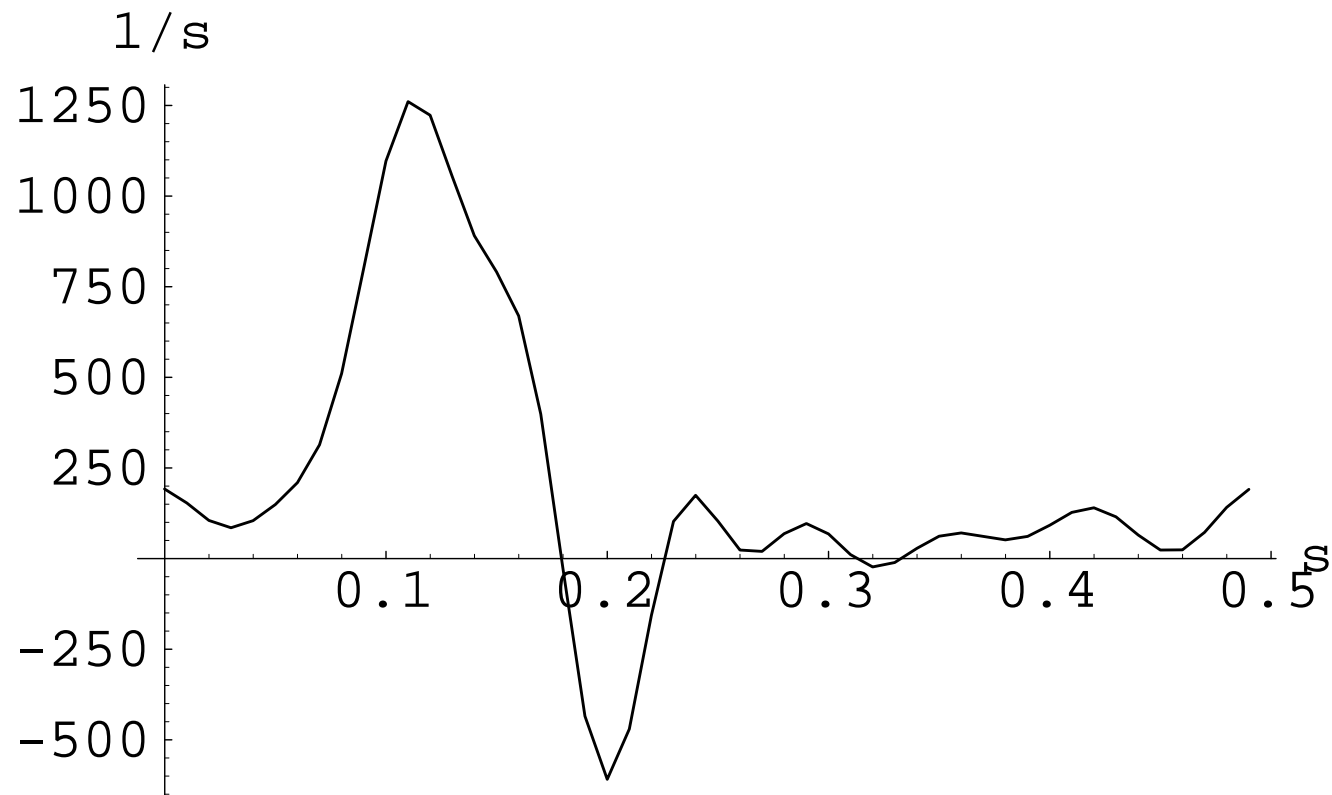


The spatial distribution $w(x)$ of the down-pipe shear.

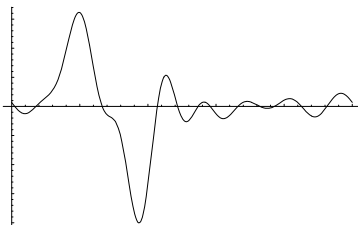
$$\sigma_H(\mathbf{x}, t) = \bar{\sigma}_H(t)w(x) + \tilde{\sigma}$$

where x is circumferential distance from the outer bend.

Wall shear time dependence $\bar{\sigma}(t)$

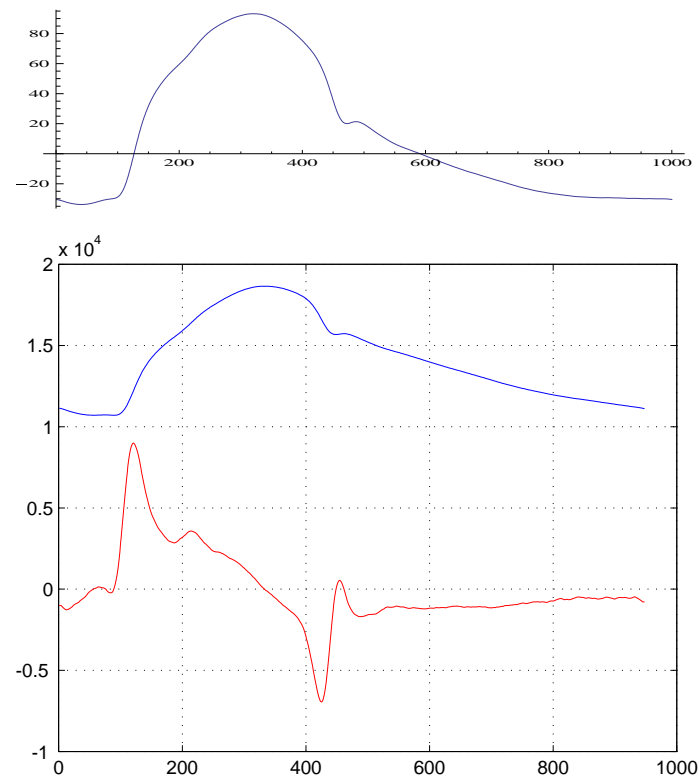


Time dependence of the down-pipe component of the wall shear rate for $\varepsilon = 1$, $b = 2.5$ and $M = 20kg$. Compare the shape of the pressure gradient:



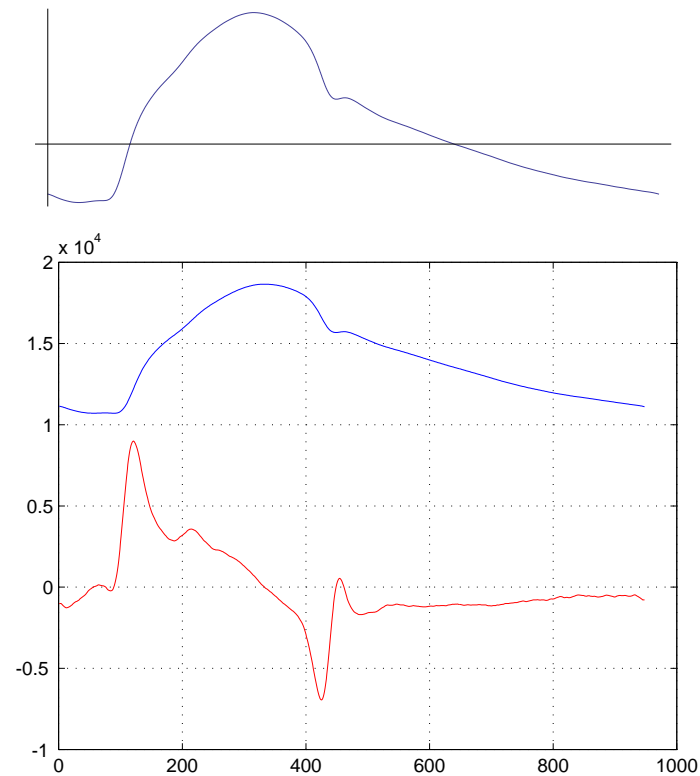
Time dependence of Computed flux

Despite the complexity of the flows, the net flux $\bar{v}(t)$ is similar in shape to the pressure, e.g. for rat $M = 0.6$



Time dependence of Computed flux

Despite the complexity of the flows, the net flux $\bar{v}(t)$ is similar in shape to the pressure, e.g. **for dog $M = 20$**



Conclusions

- Helical pipes have a more equitable wall shear, mainly by avoiding the static separation point of the secondary flow. Especially important for cross-pipe shear component. The constant swirling keeps separated structures close to the wall.

Conclusions

- Helical pipes have a more equitable wall shear, mainly by avoiding the static separation point of the secondary flow. Especially important for cross-pipe shear component. The constant swirling keeps separated structures close to the wall.
- The isotropic model leads to more severe behaviour at high M . Peak velocity increases slightly with M . For moderate M , $v' < 1m/s$. The anisotropic model predicts the peak value well and has more backflow.

Conclusions

- Helical pipes have a more equitable wall shear, mainly by avoiding the static separation point of the secondary flow. Especially important for cross-pipe shear component. The constant swirling keeps separated structures close to the wall.
- The isotropic model leads to more severe behaviour at high M . Peak velocity increases slightly with M . For moderate M , $v' < 1m/s$. The anisotropic model predicts the peak value well and has more backflow.
- Effects of pipe torsion more important in relatively slow diastolic phase. Lower values of R_s in anisotropic model contribute to this.